Lipid Membranes

Simultaneous In Situ Quantification of Two Cellular Lipid Pools Using Orthogonal Fluorescent Sensors**

Shu-Lin Liu, Ren Sheng, Matthew J. O'Connor, Yang Cui, Youngdae Yoon, Svetlana Kurilova, Daesung Lee, and Wonhwa Cho**

Abstract: *Lipids regulate a wide range of biological activities. Since their local concentrations are tightly controlled in a spatiotemporally specific manner, the simultaneous quantification of multiple lipids is essential for elucidation of the complex mechanisms of biological regulation. Here, we report a new method for the simultaneous in situ quantification of two lipid pools in mammalian cells using orthogonal fluorescent sensors. The sensors were prepared by incorporating two environmentally sensitive fluorophores with minimal spectral overlap separately into engineered lipid-binding proteins. Dual ratiometric analysis of imaging data allowed accurate, spatiotemporally resolved quantification of two different lipids on the same leaflet of the plasma membrane or a single lipid on two opposite leaflets of the plasma membrane of live mammalian cells. This new imaging technology should serve as a powerful tool for systems-level investigation of lipid-mediated cell signaling and regulation.*

Membrane lipids are among the most important and ubiquitous regulatory molecules that control the localization, activity, and mutual interactions of a wide variety of cellular proteins.[1] Because local lipid concentrations are highly variable and may serve as activation thresholds for myriad biological processes mediated by these proteins, spatiotemporally resolved lipid quantification is essential for elucidating the diverse and complex mechanisms of biological regulation.[2] We recently developed a chemical strategy for in situ quantification of a single lipid species in live mammalian cells using a hybrid sensor constructed with an engineered lipid-binding protein and an environmentally sensitive (or solvatochromic) fluorophore (ESF).[2] Quantification of cellular phosphatidylinositol-4,5-bisphosphate (PIP$_2$) by ratiometric imaging analysis demonstrated the spatiotemporal dynamics of this important signaling lipid in unprecedented detail and provided new insight into how it regulates such diverse biological processes.[2]

Under physiological conditions, multiple regulatory lipids are metabolically and functionally linked to one another.[3] Also, a single lipid species can exist disproportionally in opposite faces of lipid bilayers, performing distinct functions.[4] Most notably, the tightly controlled trans-bilayer asymmetry of lipids in the plasma membrane (PM) of mammalian cells is crucial for cell survival, function, and regulation.[4] Thus, a new technology is needed for the simultaneous in situ quantification of multiple lipids in the same membrane leaflet or a lipid species in opposite leaflets of cell membranes. As a first step toward the simultaneous quantification of multiple lipids, we developed a new strategy for dual in situ lipid quantification in live cells.

Simultaneous dual-lipid quantification would require orthogonal lipid sensors that allow robust dual ratiometric analysis. Unfortunately, the limited availability of amphiphilic ESFs greatly hampers the development of orthogonal lipid sensors. We therefore searched for an ESF that can be used orthogonally with the most commonly employed thiol-reactive amphiphilic ESF, acrylodan (6-acryloyl-2-dimethylaminonaphthalene).[5] When coupled to a cysteine residue of a protein, the 2-dimethylaminonaphthaloyl (DAN) group undergoes a green-to-blue spectral shift with a large increase in fluorescence emission intensity as the protein binds its cognate lipid in the membrane, allowing robust ratiometric quantification of cellular lipids through in vitro calibration.[2] An ideal orthogonal ESF partner for DAN would be an amphiphilic fluorescence dye that shows a spectral shift from red to orange fluorescence upon lipid binding. Among reported red fluorophores, Nile Red possesses such properties and its maleimide derivatives have been prepared for cysteine labeling.[6] These Nile Red derivatives are, however, highly lipophilic and have extremely low water solubility. This not only lowers the yield of protein-labeling reactions in aqueous solution but also adversely affects the structure, stability, and membrane-binding properties of the labeled proteins. To overcome these major limitations, we designed and synthesized several cysteine-specific acrylate derivatives of Nile Red with a varying degree of lipophilicity.

The 2-hydroxy Nile Red benzophenoxazinone core 2-HONR was synthesized starting from 5-diethylamino-2-nitrosophenol hydrochloride and 1,6-dihydroxynaphthalene (Scheme 1).[7] The first-generation fluorophore NR1 was prepared by treatment of 2-HONR with acryloyl chloride and triethylamine. Although NR1 displayed favorable spectral properties, its solubility in water was still extremely low and thus its protein-labeling efficiency was low. We thus introduced more oxygen atoms and an additional hydroxy group into the linker to increase the water solubility. NR2

[*] Dr. S.-L. Liu, Dr. R. Sheng, M. J. O'Connor, Y. Cui, Dr. Y. Yoon,[+]
    S. Kurilova, Dr. D. Lee, Dr. W. Cho
    Department of Chemistry, University of Illinois at Chicago
    845 W. Taylor St., Chicago, IL (USA)
    E-mail: dsunglee@uic.edu
            wcho@uic.edu

[+] Present address:
    Department of Environmental Health Science, Konkuk University
    1 Hwayang-dong, Gwangjin-gu, Seoul 143-701 (Korea)
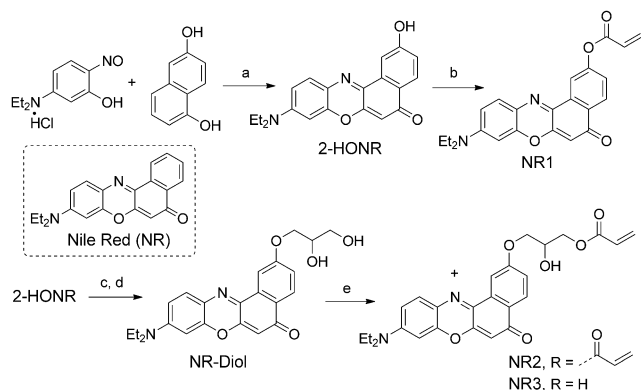
Scheme 1. Synthesis of Nile Red derivatives with an acrylate linker: a) DMF, reflux, 69%; b) acryloyl chloride (1.2 equiv), Et$_3$N (1.5 equiv), 0°C, CH$_2$Cl$_2$, 30 min, 85%; c) NaH (1.25 equiv), DMF, 0°C, 30 min; allyl bromide (2.5 equiv), 0°C to RT, 3 h, 72%; d) OsO$_4$ (cat.), NMO (2 equiv), acetone/H$_2$O/MeOH (4:1:0.5), 65%; e) acryloyl chloride (0.33 equiv), Et$_3$N (1.5 equiv), −30°C, CH$_2$Cl$_2$, 10 min, 25%. DMF = N,N-dimethylformamide, NMO = N-methylmorpholine N-oxide.

(bisacrylate) and NR3 (monoacrylate) were synthesized from the common precursor 2-HONR by a three-step sequence involving allylation, dihydroxylation, and acrylation.

Among these derivatives, NR3 afforded the highest coupling yield to the engineered ENTH domain (eENTH) that was previously used for the PIP$_2$ sensor.[2] Also, the eENTH labeled with NR3 (NR3-eENTH) had the most favorable properties, including the lowest tendency to self-associate in solution and to nonspecifically adsorb to lipid membranes and glass surfaces. Furthermore, NR3-eENTH showed a large PIP$_2$ concentration-dependent spectral shift from red to orange-red when it bound to PIP$_2$-containing vesicles (Figure S1a in the Supporting Information). A minimal spectral overlap between NR3-eENTH and DAN-eENTH (Figure S1b in the Supporting Information) suggests that DAN and NR3 may be used for preparing orthogonal lipid sensors.

To test this notion, we prepared DAN- and NR3-labeled phosphatidylserine (PS) sensors and simultaneously measured the concentrations of PS in the inner (cytofacial) and the outer (exofacial) leaflets of the PM of mammalian cells. PS is a major lipid component of PM and is predominantly found in the inner leaflet under normal conditions.[8] It is, however, translocated to the outer leaflet by the action of a Ca^{2+}-dependent scramblase during apoptosis and blood vessel damage and triggers phagocytosis and the blood coagulation cascade, respectively.[8] Currently, little is known about the spatiotemporal dynamics of PS across the PM under physiological conditions mainly because current optical imaging technologies do not allow simultaneous in situ quantification of PS in the two leaflets of the PM.

To prepare orthogonal PS sensors, we first engineered the lactadherin C2 domain (eLactC2), the fluorescence-protein-tagged forms of which have been widely used as a specific cellular PS probe,[9] to introduce a single cysteine in its membrane-binding surface. We then labeled it with acrylodan and NR3 to obtain DAN-eLactC2 and NR3-eLactC2, respec-

tively. Both DAN-eLactC2 and NR3-eLactC2 showed characteristic spectral changes upon binding to vesicles in a PS concentration-dependent manner (Figure 1 a,b). After performing in vitro ratiometric calibration of these PS sensors using giant unilamellar vesicles containing varying concentrations of PS (Figure 1 c,d; see the Supporting Information for details), we microinjected DAN-eLactC2 into NIH 3T3 cells and added NR3-eLactC2 to the medium (or vice versa). We then triggered the cell apoptosis with 1 μM doxorubicin, and simultaneously monitored DAN-eLactC2 and NR3-eLactC2 bound to the PM by a four-channel two-photon microscope equipped with two femtosecond-pulsed laser sources.

No current light microscopy, including super-resolution microscopy, allows spatial resolution of the two lipid layers of cell membranes (ca. 5 nm thick).[10] Because our PS sensors
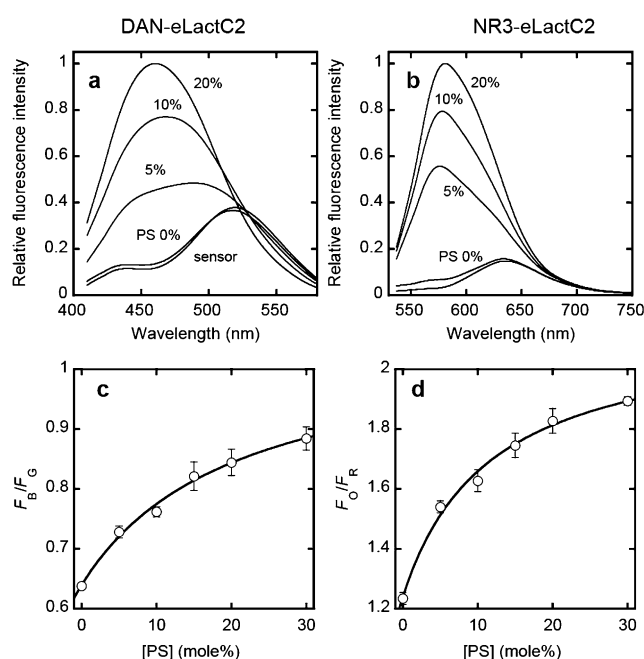

Figure 1. a–d) Spectral properties of and ratiometric calibration for orthogonal PS sensors. a,b) Fluorescence emission spectra of DAN-eLactC2 (a) and NR3-eLactC2 (b) (both 500 nM) in the presence of phosphatidylcholine (PC)/PS (100−x:x) large vesicles measured spectrofluorometrically. Numbers (x) indicate mole% of PS. The excitation wavelength was 392 nm for DAN-eLactC2 and 520 nm for NR3-eLactC2. Both exhibited a dramatic blue shift upon PS binding. c,d) Ratiometric calibration curves of DAN-eLactC2 (c) and NR3-eLactC2 (d) for PS quantification. The PS sensors were monitored by a two-photon microscope in the presence of PC/PS (100−x:x) giant vesicles. Nonlinear least-squares analysis of the plot using the equation (for DAN-eLactC2); $F_B/F_G = (F_B/F_G)_{max}/(1+K_d/[PS])+C$ yields K_d, $(F_B/F_G)_{max}$, and C values and the calibration curves are constructed using these parameters. F_B, F_G, F_o, and F_R indicate fluorescence intensities of the blue, green, orange, and red channels, respectively. K_d, $(F_B/F_G)_{max}$, and C are the equilibrium dissociation constant (in mole%), the maximal F_B/F_G value, and the arbitrary instrumental parameter. Blue and orange channels depict membrane-bound sensors whereas green and red channels show membrane-bound plus free sensors. Error bars indicate standard deviations calculated from at least three independent sets of measurements. 20 mM Tris buffer, pH 7.4, containing 0.16 M KCl was used for all measurements.

cannot cross the PM,[2] however, we were able to unambiguously distinguish the signals from the outer and the inner PM by analyzing fluorescence signals from four discrete optical channels in a time-dependent manner (Figure 2a). The slow rate of apoptosis and major changes in cell size and shape
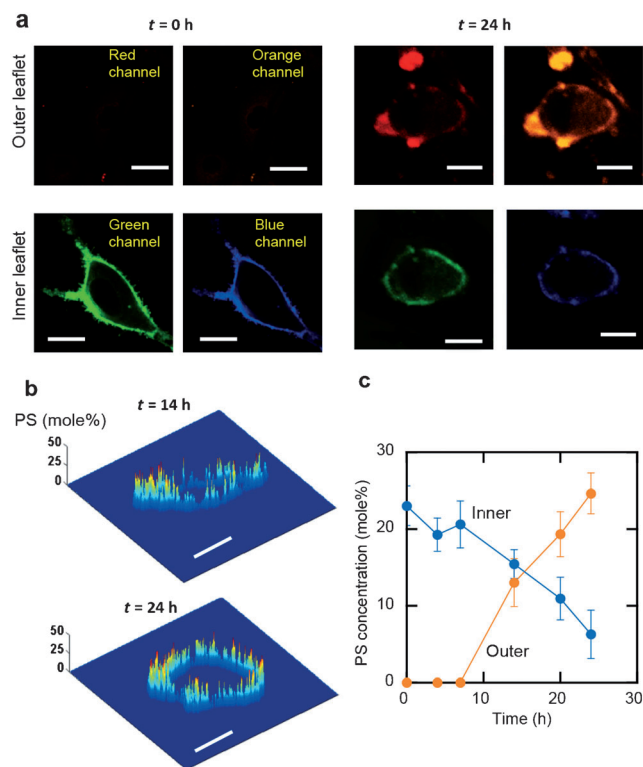

Figure 2. a–c) Simultaneous in situ quantification of PS in the inner and outer PM of NIH 3T3 cells. a) Four-channel images of representative apoptotic cells at two time points. PS in the inner and outer PM was monitored using microinjected DAN-eLactC2 (green and blue channels) and media-added NR3-eLactC2 (red and orange channels) sensors, respectively. Blue and orange channels depict membrane-bound sensors whereas green and red channels show membrane-bound plus free sensors. b) Time-lapse PS quantification in the outer PM at 14 h and 24 h. After apoptosis was induced by 1 μm doxorubicin, PS in the outer and the inner PM was quantified from the blue/green and orange/red ratios, respectively, using the ratiometric calibration curves (Figure 1c,d). c) Time-dependent changes of spatially averaged PS concentrations in the outer and inner PM. Scale bars indicate 5 μm.

during the process (Figure 2a) made continuous imaging analysis impractical. We therefore performed time-lapse imaging and data analysis. Figure 2b depicts PS quantification in the outer PM of apoptotic NIH 3T3 cells after 14 and 24 h of doxorubicin treatment. The analysis reveals for the first time pronounced local heterogeneity of PS in the outer leaflet of the PM. This implies that PS locally enriched beyond a threshold level in the outer PM may constitute hot spots for the recognition of apoptotic cells by phagocytes as seen with PIP$_2$.[2] This notion is also consistent with the finding that although PS started to appear in the outer PM after 8 h (Figure 2c), the cells showed apoptotic phenotypes (e.g., shape changes) only after 20 h. Furthermore, an excellent

correlation was seen between the increase in PS in the outer PM and its decrease in the inner PM (both spatially averaged) at a given time (Figure 2c), showing that the PS concentration increase in the outer PM is due to direct trans-bilayer translocation of PS from the inner PM. Collectively, these results not only demonstrate the feasibility of our orthogonal lipid sensor technology but also shed new light on the trans-bilayer movement of PS and its local distribution. The same experimental approach can be applied to the real-time quantification of other lipid species (e.g., cholesterol, sphingomyelin, etc.) across the PM, which should provide important new insight into the trans-bilayer dynamics and the location-specific functions of many vital cellular lipids.

Having established the feasibility of our orthogonal lipid sensor methodology, we then performed simultaneous quantification of two metabolically linked signaling lipids, PIP$_2$ and phosphatidylinositol-3,4,5-trisphosphate (PIP$_3$). PIP$_3$ is produced from PIP$_2$ in the cytofacial leaflet of the PM by phosphoinositide 3-kinase (PI3K) in response to stimuli, such as growth factors,[11] and is converted back to PIP$_2$ by a tumor suppressor lipid phosphatase, PTEN.[12] PIP$_2$ mediates a wide range of cellular processes, including cell signaling,[3a, 13] while PIP$_3$ activates myriad of other cellular activities, including cell growth.[11] Under normal conditions, PIP$_3$ is thought to exist in much lower concentration than PIP$_2$ and only transiently because PI3K activation is tightly regulated.[14] Interestingly, it has been recently reported that some mammalian cells may have significant basal levels of PIP$_3$ in the PM.[15] This in turn suggests that the PIP$_3$-to-PIP$_2$ ratio may significantly vary among different mammalian cells, greatly affecting their basal cell activities and responses to various stimuli. The PIP$_3$-to-PIP$_2$ ratio, however, has not been accurately measured in live cells.

We thus simultaneously quantified PIP$_2$ and PIP$_3$ in different mammalian cells using orthogonal sensors for PIP$_2$ and PIP$_3$. As a PIP$_3$ sensor, we engineered the PIP$_3$-selective tandem pleckstrin homology (PH) domains of myosin X (eMyoXPH)[16] for single-site cysteine labeling (see the Supporting Information for details), labeled the engineered protein with NR3 (NR3-eMyoXPH), and measured its spectral properties upon binding to PIP$_3$-containing vesicles (Figure S2 in the Supporting Information). This protein was selected over other PIP$_3$-selective PH domains, including BTK and Grp1 PH domains,[15b] because none of the latter exhibited desired spectral properties when labeled with acrylodan or NR3. NR3-labeled eMyoXPH and DAN-eENTH were then co-microinjected into NIH 3T3 cells and PIP$_2$ and PIP$_3$ were simultaneously quantified by dual ratiometric analysis of images (Figure 3a) before and after stimulation by insulin that activates PI3K.[17]

At a given time, both PIP$_2$ and PIP$_3$ exhibited a high degree of local heterogeneity (Figure 3b). Interestingly, a good spatial correlation was detected between the decrease in PIP$_2$ concentration and the increase in PIP$_3$ concentration (Figure 3c), indicating localized conversion of PIP$_2$ to PIP$_3$ and segregation of the two lipids. When spatially averaged at a given time, the PIP$_3$-to-PIP$_2$ ratio was 0.25 ± 0.05 (average ± standard deviation (S.D) in 15 cells) in the resting NIH 3T3 cells, demonstrating the significant basal PI3K activity in
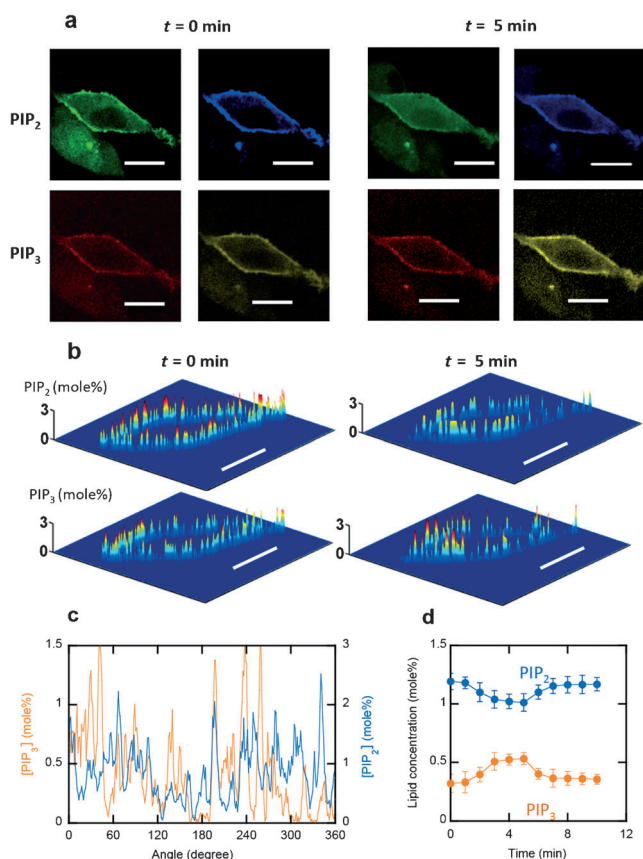
Figure 3. a–d) Simultaneous in situ quantification of PIP_2 and PIP_3 in the inner PM of NIH 3T3 cells. a) Four-channel images of representative NIH 3T3 cells before and 5 min after insulin treatment. PIP_2 and PIP_3 were monitored using microinjected DAN-eENTH and NR3-eMyoXPH, respectively. Blue and orange channels depict membrane-bound sensors whereas green and red channels show membrane-bound plus free sensors. b) PIP_2 and PIP_3 were quantified through ratiometric calibration (see Figure S2). c) Angular profiles of PIP_2 and PIP_3 in the PM 3 min after insulin treatment. PIP_2 and PIP_3 show pronounced spatial heterogeneity but a good reciprocal spatial correlation was observed between them. d) Time-dependent changes of spatially averaged PIP_2 and PIP_3 concentrations in the PM. Scale bars indicate 5 μm.

Figure 4. a, b) The PIP_3-to-PIP_2 ratio in PC cell lines. a) Time-dependent changes of spatially averaged PIP_2 and PIP_3 concentrations in the PM of PC3 cells lacking PTEN. b) Time-dependent changes of spatially averaged PIP_2 and PIP_3 concentrations in the PM of PC3 cells with transiently expressing PTEN.

these cells. The ratio reached 0.5 within 5 min of insulin stimulation and rapidly returned to the basal level (Figure 3 d).

To examine to which degree the PIP_3-to-PIP_2 ratio varies among mammalian cells, we measured the ratio in PTEN-deficient human prostate cancer cell lines, PC3 cells. The spatially averaged ratio in resting PC3 cells (i.e., 0.30 ± 0.05 in 20 cells) was only slightly higher than that in NIH 3T3 cells (Figure 4 a), indicating that the basal PI3K activity is similar in NIH 3T3 and PC3 cells. A main difference was, however, that after insulin stimulation the ratio continued to increase (> 3.0) for up to 10 min (Figure 4 a) and caused local enrichment of PIP_3 over PIP_2 (Figure S3). This result demonstrates how PTEN deletion causes irreversible activation of PIP_3 signaling, leading to cancer. When PTEN was reintroduced to PC3 cells by transient transfection, the PIP_3-to-PIP_2 ratio regained the bell-shaped time dependence after insulin
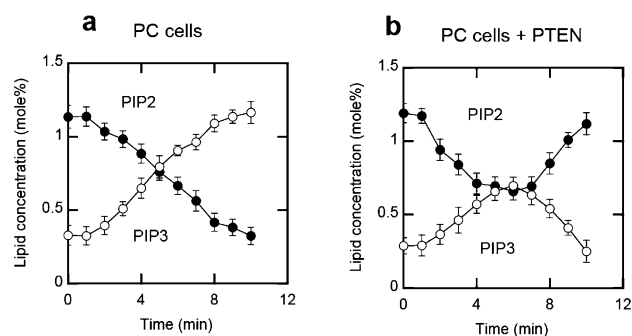
treatment (Figure 4 b), verifying that PTEN is directly responsible for the PIP_3-to-PIP_2 transition under these conditions. Taken together, these results show that PIP_2 and PIP_3 are locally metabolized by PI3K and PTEN at the PM and that the same stimulus can induce different changes in the PIP_3-to-PIP_2 ratio, depending on the cell type. This information should be essential for understanding the basis of differential regulatory mechanisms for PIP_3 signaling in mammalian cells.

In this study, we demonstrate the feasibility of our new orthogonal lipid sensor technology. Our method allows robust and simultaneous in situ quantification of two lipid pools in living mammalian cells in a spatiotemporally resolved manner. The study also shows that simultaneous quantification of two lipid pools provides physiologically important data and new insight unattainable by conventional methodologies. Collectively, it represents an important technical advance toward the systems-level analysis and understanding of complex lipid-mediated cell regulation.

[1] a) Y. A. Hannun, L. M. Obeid, *Nat. Rev. Mol. Cell Biol.* **2008**, *9*, 139–150; b) W. Cho, *Sci. STKE* **2006**, pe7; c) Y. Chen, R. Sheng, M. Kallberg, A. Silkov, M. P. Tun, N. Bhardwaj, S. Kurilova, R. A. Hall, B. Honig, H. Lu, W. Cho, *Mol. Cell* **2012**, *46*, 226–237.
[2] Y. Yoon, P. J. Lee, S. Kurilova, W. Cho, *Nat. Chem.* **2011**, *3*, 868–874.
[3] a) G. Di Paolo, P. De Camilli, *Nature* **2006**, *443*, 651–657; b) M. A. De Matteis, A. Godi, *Nat. Cell Biol.* **2004**, *6*, 487–492; c) M. G. Roth, *Physiol. Rev.* **2004**, *84*, 699–730.
[4] G. van Meer, *Cold Spring Harbor Perspect. Biol.* **2011**, *3*.
[5] G. Weber, F. J. Farris, *Biochemistry* **1979**, *18*, 3075–3078.
[6] a) S. L. Black, W. A. Stanley, F. V. Filipp, M. Bhairo, A. Verma, O. Wichmann, M. Sattler, M. Wilmanns, C. Schultz, *Bioorg. Med. Chem.* **2008**, *16*, 1162–1173; b) S. Y. Kim, A. N. Semyonov, R. J. Twieg, A. L. Horwich, J. Frydman, W. E. Moerner, *J. Phys. Chem. B* **2005**, *109*, 24517–24525; c) O. A. Kucherak, S. Oncul,

Z. Darwich, D. A. Yushchenko, Y. Arntz, P. Didier, Y. Mely, A. S. Klymchenko, *J. Am. Chem. Soc.* **2010**, *132*, 4907–4916; d) A. Okamoto, K. Tainaka, Y. Fujiwara, *J. Org. Chem.* **2006**, *71*, 3592–3598; e) O. Wichmann, C. Schultz, *Chem. Commun.* **2001**, 2500–2501; f) B. E. Cohen, A. Pralle, X. Yao, G. Swaminath, C. S. Gandhi, Y. N. Jan, B. K. Kobilka, E. Y. Isacoff, L. Y. Jan, *Proc. Natl. Acad. Sci. USA* **2005**, *102*, 965–970.

[7] M. S. J. Briggs, I. Bruce, J. N. Miller, C. J. Moody, A. C. Simmonds, E. Swann, *J. Chem. Soc. Perkin Trans. 1* **1997**, 1051–1058.

[8] P. A. Leventis, S. Grinstein, *Annu. Rev. Biophys.* **2010**, *39*, 407–427.

[9] T. Yeung, G. E. Gilbert, J. Shi, J. Silvius, A. Kapus, S. Grinstein, *Science* **2008**, *319*, 210–213.

[10] B. Huang, M. Bates, X. Zhuang, *Annu. Rev. Biochem.* **2009**, *78*, 993–1016.

[11] a) B. Vanhaesebroeck, J. Guillermet-Guibert, M. Graupera, B. Bilanges, *Nat. Rev. Mol. Cell Biol.* **2010**, *11*, 329–341; b) B. Vanhaesebroeck, L. Stephens, P. Hawkins, *Nat. Rev. Mol. Cell Biol.* **2012**, *13*, 195–203.

[12] C. A. Worby, J. E. Dixon, *Annu. Rev. Biochem.* **2014**, *83*, 641–669.

[13] a) S. McLaughlin, D. Murray, *Nature* **2005**, *438*, 605–611; b) S. McLaughlin, J. Wang, A. Gambhir, D. Murray, *Annu. Rev. Biophys. Biomol. Struct.* **2002**, *31*, 151–175.

[14] L. C. Cantley, *Science* **2002**, *296*, 1655–1657.

[15] a) W. D. Heo, T. Inoue, W. S. Park, M. L. Kim, B. O. Park, T. J. Wandless, T. Meyer, *Science* **2006**, *314*, 1458–1461; b) D. Manna, N. Bhardwaj, M. S. Vora, R. V. Stahelin, H. Lu, W. Cho, *J. Biol. Chem.* **2008**, *283*, 26047–26058.

[16] Q. Lu, J. Yu, J. Yan, Z. Wei, M. Zhang, *Mol. Biol. Cell* **2011**, *22*, 4268–4278.

[17] N. B. Ruderman, R. Kapeller, M. F. White, L. C. Cantley, *Proc. Natl. Acad. Sci. USA* **1990**, *87*, 1411–1415.